Coupled Ultrafast Lattice and Polarization Dynamics in Ferroelectric Nanolayers

C. v. Korff Schmising,[1] M. Bargheer,[1,*] M. Kiel,[1] N. Zhavoronkov,[1] M. Woerner,[1] T. Elsaesser,[1]
I. Vrejoiu,[2] D. Hesse,[2] and M. Alexe[2]

[1]*Max-Born-Institut für Nichtlineare Optik und Kurzzeitspektroskopie, Max-Born-Strasse 2a, 12489 Berlin, Germany*
[2]*Max-Planck-Institut für Mikrostrukturphysik, Weinberg 2, 06120 Halle, Germany*

(Received 21 December 2006; published 18 June 2007)

We report the first analysis of the polarization and lattice dynamics in a metal/ferroelectric/metal nanolayer system by femtosecond x-ray diffraction. Two Bragg reflections provide information on the coupled dynamics of the two relevant phonon modes for ferroelectricity in perovskites, the tetragonal distortion and the soft mode. Optical excitation of the $SrRuO_3$ metal layers generates giant stress ($>$ 1 GPa) compressing the $PbZr_{0.2}Ti_{0.8}O_3$ layers by up to 2%. The resulting change of tetragonality reaches a maximum after 1.3 ps. As a result, the ferroelectric polarization P is reduced by up to 100% with a slight delay that is due to the anharmonic coupling of the two modes.

DOI: 10.1103/PhysRevLett.98.257601 PACS numbers: 77.84.Lf, 61.10.Nz, 73.40.Sx, 77.80.−e

Correlations of electrons and ionic charges play a fundamental role in solid state physics and lead to phenomena such as ferroelectricity, superconductivity, and (anti)ferromagnetism. In the perovskite crystal structure the different distributions of charges lead to ferroelectric [e.g., $PbZr_xTi_{1-x}O_3$ (PZT)], dielectric [e.g., $SrTiO_3$ (STO)], and metallic properties [e.g., $SrRuO_3$ (SRO)]. The recent progress in the growth of nanostructures from these materials allows for tailoring and controlling the ferroelectric properties [1–3]. So far, most research has concentrated on the *static* characterization of the dielectric and structural properties of such nanostructures [4,5], aiming at a reduced lower limit in film thickness that sustains ferroelectric polarizations by epitaxial strain engineering [6,7] or by screening the depolarization field in sandwiched geometries [8–11].

The ferroelectric properties of $PbTiO_3$ (PTO) and its derivatives like PZT solid solutions are essentially determined and controlled by two prominent phonon modes of the crystal lattice [12] as explained in Fig. 1(a). (i) The tetragonal distortion along the c axis is characterized by the tetragonality $\eta = c/a$ of the unit cell where a and c are the in-plane and out-of-plane lattice constants of a c-axis oriented film [10]. (ii) The ferroelectric soft mode is connected with the displacement $\xi_{\text{Pb-Ti}} = \xi_{\text{Pb-O}} - \xi_{\text{Ti/Zr-O}}$ of the Pb and Ti cations given by the difference of the displacements between the respective cation and the oxygen anions. The ferroelectric polarization P is proportional to the soft mode displacement, i.e., $P \propto \xi_{\text{Pb-Ti}}$. At room temperature, the underdamped soft mode displays a frequency somewhat below 100 cm^{-1}, corresponding to a subpicosecond oscillation period [13].

The equilibrium values of η and $\xi_{\text{Pb-Ti}}$ in a nanostructure depend critically on various external parameters, namely, temperature, external stress, screening, etc., and are determined by the minimum of the strongly anharmonic potential surface along the two prominent modes sketched in Fig. 1(c) [12]. In particular, the effective crystal Hamiltonian [14] contains a term proportional to $\eta\xi^2_{\text{Pb-Ti}}$ which connects the equilibrium values of η and $\xi_{\text{Pb-Ti}}$ via the approximative relation

$$(\xi_{\text{Pb-Ti}}/\xi_0)^2 = (\eta - \eta_C)/\eta_0 \qquad (1)$$

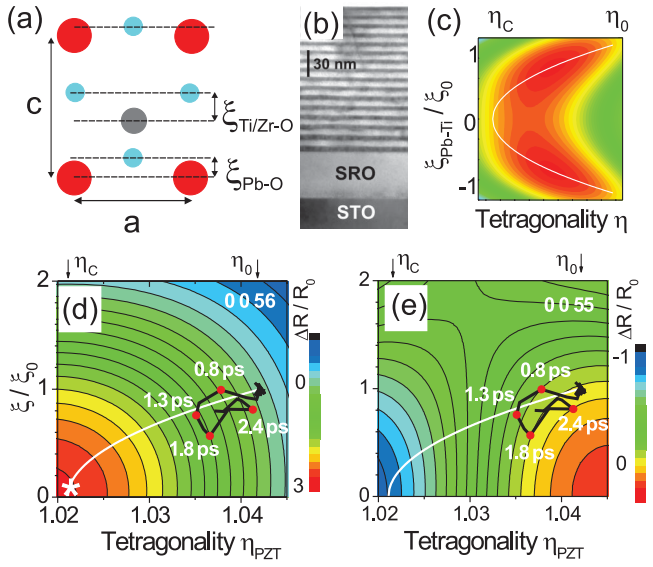

FIG. 1 (color). (a) Tetragonal strain $\eta = c/a$ and ferroelectric ion displacements $\xi_{\text{Ti/Zr-O}}$ and $\xi_{\text{Pb-O}}$ in the unit cell of PZT. (b) TEM image of a thinned PZT/SRO SL. (c) Schematic anharmonic potential energy surface as a function of η and $\xi_{\text{Pb-Ti}}$ (contour plot). The minimum of the potential lies on the white line [equilibrium $\xi_{\text{Pb-Ti}}(\eta) = \xi_{\text{Pb-O}} - \xi_{\text{Ti/Zr-O}}$, Eq. (1)]. The initial values (η_0, ξ_0) and the critical tetragonality η_C for which $\xi_{\text{Pb-Ti}} = 0$ are indicated. (d) Contour plot of the calculated change of the (0 0 56) reflectivity as a function of the tetragonality η and the relative ion displacement ξ/ξ_0. Black line: trajectory derived from Fig. 2(b) with red dots indicating selected time delays. (e) Calculated reflectivity change of (0 0 55) as a function of η and ξ.

 © 2007 The American Physical Society

with the initial values η_0, ξ_0 and the critical tetragonality η_C of PZT where the soft mode elongation vanishes due to the dynamic compression. This relation is plotted as a white line in the contour plots of Figs. 1(c)–1(e) for the sample studied here. A change of the external stress gives rise to a changed anharmonic potential with a new minimum on the white line [Fig. 1(c)].

The ferroelectric polarization of thin films has been determined both by piezoresponse measurements [10,15] and by structure analysis of the ionic displacements based on diffraction methods [16]. Recently, most accurate results were obtained by x-ray diffraction measurements of the tetragonality $\eta = c/a$ in nanolayered structures [6,10]. Such *static* investigations show that for thin $PbTiO_3$ films of a few nanometers thickness, finite size effects and screening reduce the tetragonality to $\eta_0 = 1.05$ and that for a thickness of 1 nm the polarization vanishes ($\eta_C = 1.03$) [10].

The *dynamics* of ferroelectricity is intrinsically coupled to lattice dynamics, i.e., atomic motions along the two modes η and $\xi_{\text{Pb-Ti}}$. This raises the question if and how fast the macroscopic polarization of perovskite nanolayers can be manipulated by launching lattice excitations. So far, experimental work on this important issue has remained limited. All-optical measurements of the ultrafast polarization dynamics lack the exact determination of atomic amplitudes, and the fastest switching times observed so far for epitaxial ferroelectrics are in the 100 ps range [17]. In this Letter, we apply ultrafast x-ray diffraction with a 100 fs temporal and a picometer spatial resolution to study polarization dynamics in a $PbZr_{0.2}Ti_{0.8}O_3/SrRuO_3$ superlattice (SL) under optically induced uniaxial stress. Two Bragg reflections provide sufficient information to derive the coupled dynamics of the two modes that are relevant for ferroelectricity. The uniaxial stress compresses the PZT layers by up to $\Delta\eta/\eta_0 = 0.022$ without destroying the sample. We demonstrate that such transient stress can reversibly switch off the ferroelectric polarization of PZT within less than 2 ps. This represents the first real-time observation of ultrafast structural dynamics in ferroelectric nanostructures.

The PZT/SRO SL sample studied here was fabricated by pulsed-laser deposition [18]. A $SrRuO_3$ bottom electrode layer of ≈ 60 nm thickness was deposited on a vicinal single crystalline $SrTiO_3$ substrate, and $N = 15$ periods of $d_{\text{PZT}} \approx 5$ nm thick PZT and $d_{\text{SRO}} \approx 6$ nm thick SRO layers were grown on top with their c axis parallel to the SL stacking axis. A cross-section transmission electron micrograph of a thinned fraction of the sample is shown in Fig. 1(b).

The measured stationary x-ray reflectivity (green line) and a simulation based on dynamic x-ray diffraction theory (black line, Darwin formalism [19]) are shown in Fig. 2(a) as a function of diffraction angle. The SL structure gives substantially higher x-ray diffraction signals than a single PZT layer. The SL period $d_{\text{SL}} = d_{\text{PZT}} + d_{\text{SRO}}$ gives rise to maxima (0 0 ℓ) at Bragg angles Θ corresponding to multiples $G = \ell g_{\text{SL}}$ of the reciprocal SL vector $g_{\text{SL}} = 2\pi/d_{\text{SL}}$. From the angular positions and intensities of the Bragg peaks, we derive the following structural parameters averaged over the equilibrium SL structure: $d_{\text{SL}} = 11.2$ nm, $d_{\text{SRO}} = 6.29$ nm, $d_{\text{PZT}} = 4.92$ nm, $c_{\text{SRO}} = 0.393$ nm, $c_{\text{PZT}} = 0.410$ nm, $\xi_{\text{Ti-O}} = 0.024$ nm, $\xi_{\text{Pb-O}} = 0.038$ nm [20]. This results in $\eta_0 = 1.042$ for PZT according to the pseudomorphic growth condition dictated by the in-plane lattice constant $a_{\text{SRO}} = 0.393$ nm of the strain-relaxed SRO electrode.

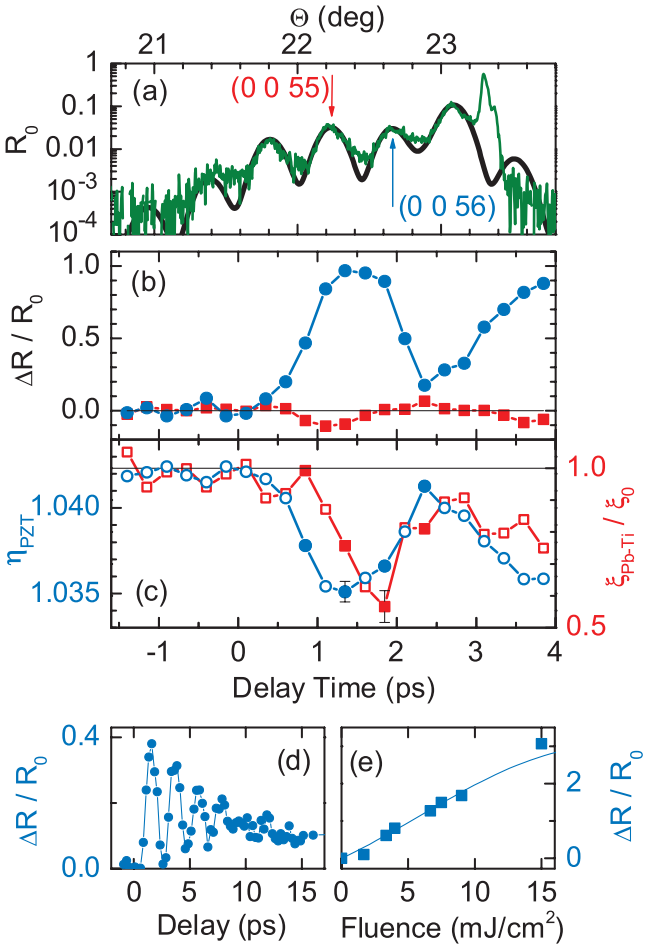

FIG. 2 (color). (a) Measured (green line) and simulated (thick black line) stationary x-ray reflectivity of the PZT/SRO SL as a function of the Bragg angle Θ. Substrate peak at 23.3°. (b) Transient change of the (0 0 56) (blue circles) and (0 0 55) (red squares) reflectivities for a pump fluence of 5 mJ/cm^2. (c) Derived transient change of the tetragonality $\eta(t)$ (blue circles) and soft mode elongation $\xi_{\text{Pb-Ti}}$ (red squares), equivalent to the trajectories in Figs. 1(d) and 1(e). Solid symbols are reproduced as dots in Figs. 1(d) and 1(e). (d) Oscillatory (0 0 56) signal with a 2 ps period on a longer time scale. (e) Fluence dependence of the peak reflectivity change of the (0 0 56) reflection around $t \approx 1.5$ ps. The solid line indicates the calculated reflectivity change according to a linear fluence dependence of the tetragonality with a ξ given by Eq. (1). For the highest fluence (15 mJ/cm^2) $\Delta R_{\text{max}}/R_0 = 3$ which implies that P approaches zero [red region in lower left corner of Fig. 1(d)].

In the femtosecond experiments, the sample is excited by a 50 fs pump pulse at 800 nm which interacts predominantly with the SRO layers, in this way generating a transient stress in the SL. The resulting lattice response is probed by an ultrashort hard x-ray pulse (Cu K_α, photon energy 8.05 keV, $\lambda = 0.154$ nm) which is diffracted from the excited sample. The experimental setup has been described in detail elsewhere [21,22]. Changes of the diffracted intensity are measured for different SL Bragg peaks as a function of pump-probe delay.

In Fig. 2(b) we show the change of the x-ray reflectivity $\Delta R/R_0$ of the SL on the (0 0 56) (blue circles) and (0 0 55) (red squares) Bragg reflections as a function of pump-probe delay for a pump fluence of 5 mJ/cm^2. Both reflectivity changes display an oscillatory time behavior, that is shown on an extended time scale in Fig. 2(d). The period of 2 ps is independent of the pump fluence. The peak reflectivity change of the (0 0 56) reflection shows a roughly linear fluence dependence [Fig. 2(e)]. The observed line shift $\Delta\Theta/\Theta_0$ of the (0 0 56) reflection as a function of delay time (Fig. 3) indicates an almost unchanged Bragg angle for delays <4 ps, followed by a shift of -0.0025 within 30 ps that remains constant up to 200 ps.

We now discuss the structural dynamics of the SL sample giving rise to the x-ray reflectivity changes shown in Figs. 2 and 3. The 50 fs pump pulse interacts primarily with the electrons in the metallic SRO layers and generates an electronic excitation spatially modulated with the SL periodicity $1/d_{\mathrm{SL}}$. Electron-phonon coupling results in a concomitant weakening of bonds in the SRO layers, in this way creating stress spatially modulated with the same periodicity. Such stress drives a SL phonon mode, i.e., a strain wave, with a wave vector g_{SL}, corresponding to the wave vector $k = 0$ in the folded Brillouin zone [21,23]. Stress is generated on a time scale short compared to the vibrational period $T = 2$ ps of the SL phonon mode and thus launches a coherent superposition of acoustic phonon states corresponding to a standing wave in the SL. This results in a modulation of the SRO and PZT layer thicknesses and—with the c axis of the layers and the SL stack axis being parallel—of the tetragonal distortions η_{SRO} and η_{PZT} with a period T. Such lattice motions are manifested in the oscillations of x-ray reflectivity as shown in Figs. 2(b) and 2(d).

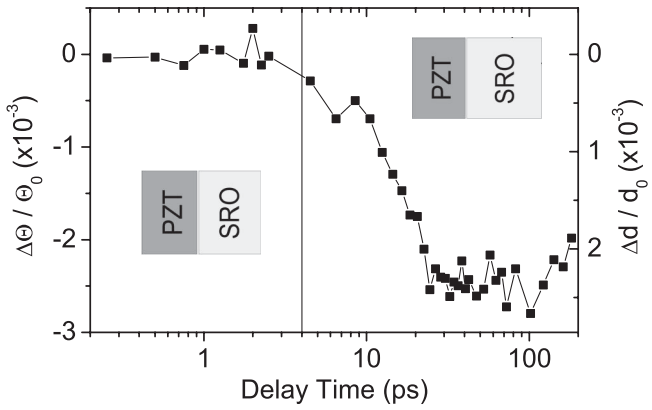

FIG. 3. Relative angular shift of the (0 0 56) Bragg reflection for an excitation fluence of 5 mJ/cm^2. Right ordinate scale: corresponding change of the SL period.

The SL Bragg peaks occur at angular positions determined by the reciprocal lattice vectors $G = lg_{\mathrm{SL}}$. The data in Fig. 3 show that such positions and, thus, d_{SL} remain unchanged during the first 4 ps after excitation. Thus, the SL oscillations during this time [Fig. 2(b)] occur with a transient expansion (compression) of the SRO layers being compensated by a compression (expansion) of the adjacent PZT layers: $\Delta\eta_{\mathrm{PZT}} = \eta_{\mathrm{PZT}} - \eta_0 = -\Delta\eta_{\mathrm{SRO}} d_{\mathrm{SRO}}/d_{\mathrm{PZT}}$. After this initial period, we observe the expansion of the entire SL structure by 0.24%. This expansion of the entire structure originates from strain fronts starting from the interfaces of the SL to air and to the substrate, where the stress is not balanced [24]. Such strain fronts propagate with the sound velocities $v_{\mathrm{PZT,SRO}}$ [25], leading to an expansion time of the entire SL ($N = 15$ periods) of $T_{\mathrm{exp}} = N d_{\mathrm{SL}}/v_{\mathrm{PZT,SRO}} \approx 30$ ps. As a result, the d_{SL} of most SL periods and, thus, the SL Bragg peak positions remain unchanged during the first 4 ps.

The anharmonic coupling of the directly driven tetragonal distortion η_{PZT} and the soft mode coordinate $\xi_{\mathrm{Pb\text{-}Ti}}$ results in a simultaneous elongation of the latter and a change of the polarization $P \sim \xi_{\mathrm{Pb\text{-}Ti}}$. Our measurements for two different Bragg peaks allow for a quantitative analysis of the microscopic lattice dynamics. To extract the momentary elongations along the two coordinates η_{PZT} and $\xi_{\mathrm{Pb\text{-}Ti}}$ from the time-resolved data, we first calculate the intensity change of the (0 0 56) and (0 0 55) SL peaks as a function of η_{PZT} and $\xi_{\mathrm{Pb\text{-}Ti}}/\xi_0$ [Figs. 1(d) and 1(e)] for constant d_{SL} as observed up to delay times of 4 ps. The intensity of the two SL peaks behaves differently as a function of the two coordinates with nearly orthogonal contour lines around $\eta_{\mathrm{PZT}} = \eta_0$ and $\xi_{\mathrm{Pb\text{-}Ti}}/\xi_0 = 1$. A specific value of $\Delta R^{56}(t)/R_0^{56}$ measured in the time-resolved experiments corresponds to a calculated contour in Fig. 1(d), and $\Delta R^{55}(t)/R_0^{55}$ corresponds to a contour in Fig. 1(e). The intersection of the two contour lines gives the values of $\eta_{\mathrm{PZT}}(t)$ and $\xi_{\mathrm{Pb\text{-}Ti}}(t)/\xi_0$ for the time t, in this way defining a trajectory in η-ξ space [black solid line in Figs. 1(d) and 1(e)].

The time dependence of η_{PZT} and $\xi_{\mathrm{Pb\text{-}Ti}}/\xi_0$ derived in this way is plotted in Fig. 2(c). The error bars are derived from the intensity fluctuations of the Bragg peaks taking into account the nonlinear transformation into η_{PZT} and $\xi_{\mathrm{Pb\text{-}Ti}}/\xi_0$. Driving the tetragonal distortion η_{PZT} generates a 50% decrease of the soft mode elongation $\xi_{\mathrm{Pb\text{-}Ti}}/\xi_0$ and, thus, of the ferroelectric polarization P on an ultrafast time scale [26]. Note that this trajectory starts close to the white line [adiabatic application of stress Eq. (1)], with significant deviations after 1.3 ps due to the dynamic coupling of the two modes. The white star in the lower left corner of Fig. 1(d) indicates the highest measured reflectivity change

$\Delta R_{\max}/R_0 = 3$ according to Fig. 2(e) (pump fluence 15 mJ/cm^2), corresponding to a complete switch off of the polarization $P \approx 0$. This defines the critical tetragonal distortion $\eta_C = 1.02$, corresponding to a peak strain $\Delta\eta/\eta_0 = 0.022$ which is achieved by a stress of 1 GPa, as estimated with the elastic constants $C_{11} = \rho v^2$ of PZT and SRO (ρ: mass densities) [25].

Detailed inspection of Fig. 2(c) demonstrates that ξ/ξ_0 reaches its maximum change approximately $\tau_P = 500 \pm 250$ fs after the maximum change of η_{PZT}, a behavior consistent with the shape of the potential energy surface [Fig. 1(c)] of the two coupled modes: Around $\eta \simeq \eta_0$ where vibrational motion starts, the narrow potential well along ξ allows for small changes of $\xi_{\mathrm{Pb\text{-}Ti}}$ with a comparably high frequency only. During the compression η reaches smaller values and the potential along ξ widens and softens, now allowing for stronger changes in this coordinate with a lower frequency. The additional delay in $\xi_{\mathrm{Pb\text{-}Ti}}$ represents the fraction of the soft mode period required to reach the maximum change.

Finally, we briefly consider the recovery of $\eta(t)$ and $\xi_{\mathrm{Pb\text{-}Ti}}(t)$ on a longer time scale. The simultaneous analysis of the measured reflectivity change and the line shift shows that even after 200 ps the excited metallic SRO is still expanded nearly 50% of the peak value, an order of magnitude more than the estimated thermal expansion ($\alpha_{\mathrm{SRO}} \approx 1.5 \times 10^{-5}$). In contrast, the PZT shows a much smaller compression which can be rationalized by the estimated temperature rise of 30 K and the negative thermal expansion coefficient of PZT ($\alpha_{\mathrm{PZT}} \approx 7 \times 10^{-5}$). The tetragonal distortion $\eta_0 = 1.042$ is restored after 30 ps and the recovery of the PZT polarization [$\xi_{\mathrm{Pb\text{-}Ti}}(30\ \mathrm{ps}) \approx \xi_0$] is directly connected to the expansion of the entire SL.

In conclusion, we have presented an ultrafast structural characterization of lattice and polarization dynamics in ferroelectric nanolayers, where a pair of Bragg reflections was chosen to derive the trajectory of the two coupled modes (η and ξ) that are relevant for the ferroelectric polarization P. Optical excitation generates stress of 1 GPa leading to a strong suppression of the ferroelectric polarization, which can even be completely switched off. Our work shows the feasibility of active ultrafast manipulation of spatial charge arrangements and electric fields in nanostructures by optically generated mechanical stress, a concept that is highly relevant for unraveling the structure-function relationship in correlated materials.

We gratefully acknowledge financial support from the Deutsche Forschungsgemeinschaft (No. SPP1134).

*bargheer@mbi-berlin.de

[1] C. H. Ahn, K. M. Rabe, and J.-M. Triscone, Science **303**, 488 (2004).
[2] R. McKee, F. Walker, and M. Chisholm, Science **293**, 468 (2001).
[3] J. F. Scott and C. A. Paz de Araujo, Science **246**, 1400 (1989).
[4] M. Dawber, K. M. Rabe, and J. F. Scott, Rev. Mod. Phys. **77**, 1083 (2005).
[5] P. Ghosez and J. Junquera, in *First Principles Modeling of Ferroelectric Oxides Nanostructures*, edited by M. Rieth and W. Schommers (American Scientific, Stevenson Ranch, CA, 2006).
[6] K. J. Choi *et al.*, Science **306**, 1005 (2004).
[7] H. N. Lee, H. M. Christen, M. F. Chisholm, C. M. Rouleau, and D. H. Lowndes, Nature (London) **433**, 395 (2005).
[8] J. Junquera and P. Ghosez, Nature (London) **422**, 506 (2003).
[9] G. Gerra, A. Tagantsev, N. Setter, and K. Parlinski, Phys. Rev. Lett. **96**, 107603 (2006).
[10] C. Lichtensteiger, J.-M. Triscone, J. Junquera, and P. Ghosez, Phys. Rev. Lett. **94**, 047603 (2005).
[11] M. Dawber and J. F. Scott, Jpn. J. Appl. Phys. **41**, 6848 (2002).
[12] R. E. Cohen, Nature (London) **358**, 136 (1992).
[13] J. A. Sanjurjo, E. Lopez-Cruz, and G. Burns, Solid State Commun. **48**, 221 (1983).
[14] U. V. Waghmare and K. M. Rabe, Phys. Rev. B **55**, 6161 (1997).
[15] *Nanoscale Characterization of Ferroelectric Materials—Scanning Probe Microscopy Approach*, edited by M. Alexe and A. Gruverman (Springer, Heidelberg, 2004).
[16] G. Shirane, R. Pepinsky, and B. C. Frazer, Acta Crystallogr. **9**, 131 (1956).
[17] Y. W. So, D. J. Kim, T. W. Noh, J.-G. Yoon, and T. Song, Appl. Phys. Lett. **86**, 092905 (2005).
[18] I. Vrejoiu, G. Le Rhun, L. Pintilie, D. Hesse, M. Alexe, and U. Gösele, Adv. Mater. **18**, 1657 (2006).
[19] S. M. Durbin and G. C. Follis, Phys. Rev. B **51**, 10 127 (1995).
[20] We assume that the lattice constants of the SRO layers in the SL agree with the value for a pseudocubic thin film $c_{\mathrm{SRO}} = 0.393$ nm [N. D. Zakharov *et al.*, J. Mater. Res. **14**, 4385 (1999)]. d_{SL} is derived from the precisely known Bragg angles. The other parameters are gained from the best fit of the theory to the data. As the oxygen atoms make a minor contribution to the diffraction pattern, similar to other structure studies [C.-L. Jia *et al.*, Nat. Mater. **6**, 64 (2007)], we assume $\xi_{\mathrm{Pb\text{-}Ti}} \propto \xi_{\mathrm{Pb\text{-}O}} \propto \xi_{\mathrm{Ti/Zr\text{-}O}}$ and use $\xi_{\mathrm{Pb\text{-}Ti}}$ as the soft mode elongation.
[21] M. Bargheer *et al.*, Science **306**, 1771 (2004).
[22] N. Zhavoronkov *et al.*, Opt. Lett. **30**, 1737 (2005).
[23] C. Colvard *et al.*, Phys. Rev. B **31**, 2080 (1985).
[24] C. v. Korff Schmising *et al.*, Phys. Rev. B **73**, 212202 (2006).
[25] The sound velocities are $v_{\mathrm{SRO}} = 6312$ m/s [S. Yamanaka *et al.*, J. Solid State Chem. **177**, 3484 (2004)] and $v_{\mathrm{PZT}} \approx 4500$ m/s [M. Kahn, J. Am. Ceram. Soc. **68**, 623 (1985)].
[26] Other polar-optical modes occurring at frequencies higher than 400 cm^{-1} [P. Ghosez *et al.*, Phys. Rev. B **60**, 836 (1999)] are not driven by the gradual buildup of stress in our experiment. Thus, the corresponding contributions to the *electric* polarization are absent.